The potential for super-Nyquist asteroseismology with *TESS*

Simon J. Murphy[1,2]⋆

[1]*Sydney Institute for Astronomy (SIfA), School of Physics, University of Sydney, NSW 2006, Australia*
[2]*Stellar Astrophysics Centre, Department of Physics and Astronomy, Aarhus University, DK-8000 Aarhus C, Denmark*

ABSTRACT

The perfect 30-min cadence of the full-frame images from the *Transiting Exoplanet Survey Satellite* (*TESS*) will impose a hard Nyquist limit of $24 \, \mathrm{d}^{-1}$ ($\approx 278 \, \mu\mathrm{Hz}$). This will be problematic for asteroseismology of stars with oscillation frequencies at or around that Nyquist limit, which will have insurmountable Nyquist ambiguities. *TESS* does offer some observing slots at shorter cadences, but these will be limited in number and competitive, while the full-frame images will be the main data product for many types of variable stars. We show that the Nyquist ambiguities can be alleviated if, when *TESS* resumes observations after a downlink, integrations are not resumed at perfect cadence with those before the downlink. The time spent idling before integrations are resumed need only be around 5 min for satisfactory results, and observing time can be recouped from the downlink event if the telescope does not wait for a return to perfect cadence before resuming integrations. The importance of imperfect cadence after downlink is discussed in light of phase coverage of transit events.

Key words: asteroseismology – techniques: photometric – stars: oscillations – stars: variable: δ Scuti – stars: variable: general.

1 INTRODUCTION

The *Transiting Exoplanet Survey Satellite* (*TESS*; Ricker et al. 2015) is due to be launched in 2018. By focusing on brighter targets than those of the *Kepler* mission and by having full sky coverage, *TESS* presents many new opportunities in the fields of exoplanets and asteroseismology.

TESS will observe in three cadences: full-frame images will be available at a strict 30-min cadence, while individual targets can be observed at 2-min and 20-s cadences. While some 200 000 stars will be observed at 2-min cadence, these will comprise mostly of cool planet-host candidates. Stars with spectral types earlier than ∼F5 will not be observed at the 2-min or 20-s cadences unless they compete successfully under guest observer or asteroseismic target programmes. In addition, supply of the 20-s cadence slots is small, and the demand is expected to be high. Hence, maximizing the utility of the 30-min cadence is important.

The sampling situation with *TESS* is not dissimilar to that of the *Kepler* mission. *Kepler* has the capability of observing in a long-cadence (LC) mode of 29.45-min and a short-cadence (SC) mode of 58.85 s (Koch et al. 2010). Only 512 SC slots are available, and because of memory and telemetry constraints, not all of these can be used in the successor mission, K2 (Howell et al. 2014).

The hard Nyquist limit of *Kepler* was overcome due to the unique features of *Kepler*'s heliocentric orbit. The full details were presented by Murphy, Shibahashi & Kurtz (2013a), but a short summary is given here. In the original mission, a ± 200-s Rømer delay existed along the telescope's line of sight towards its field of view between Cygnus and Lyra. As a result, its sampling, which was strictly regular on board the satellite, was periodically modulated by its orbit when those times were converted to barycentric Julian Date (BJD). The periodic modulation therefore applied to the Nyquist frequency. Nyquist aliases became multiplets in the Fourier transform, when the observations were longer than one *Kepler* orbit of 372.5 d, while real oscillation peaks remained as singlets. Furthermore, the distribution of power into these multiplets meant that aliases had lower amplitudes than the real peaks. The outcome was that classical pulsators were no longer plagued by Nyquist ambiguity, and the number of stars that could be analysed with confidence increased by nearly two orders of magnitude.

Application of the same methodology to *TESS* meets problems. *TESS* is in a geocentric orbit inclined to the ecliptic plane, with a period of just 13.7 d. The light-travel time across its eccentric orbit is only 1.6 s, which is far shorter than the 1800 s of one full-frame integration. As such, the modulation to the sampling will not have a detectable effect, and Nyquist ambiguities cannot be resolved in this way. A full explanation is provided in Section 3. Of course, the Earth also orbits the Sun, but *TESS* does not look at any field for one or more Earth orbits except for the continuous viewing zone within $12°$ of the ecliptic pole. Unfortunately, since the Rømer delay is the product of the light-travel time across the orbit with the cosine of the latitude of the field, the effect is small, and is applicable to only a tiny fraction of *TESS* targets.

⋆E-mail: murphy@physics.usyd.edu.au

Fortunately, an alternative solution is available. *TESS*'s step-and-stare operations continue for 27 d for each field, which equals two orbits. A data downlink occurs at each perigee, during which no observations take place. We show in this paper that the amplitudes of the Nyquist aliases are attenuated if the return to cadence after a downlink is imperfect. This allows the real oscillation frequencies, which are the fundamental data of asteroseismology, to be distinguished from their aliases.

2 NYQUIST ALIASING

Nyquist aliases are peaks in the Fourier transform of the stellar light curve that describe the data equally as well as the true peak. There are an infinite number of Nyquist aliases, and some external physical constraint is required to bound the frequency range of pulsating stars. This could be as fundamental as restricting pulsation time-scales to be longer than the light-travel time across the star, but stellar pulsation models can offer much tighter constraints. Still, the frequency ranges of some classes of variable star can straddle one or more Nyquist frequencies of the most commonly used data products, such as the light curves from *Kepler* and those anticipated from *TESS*.

Nyquist aliases are particularly problematic when the sampling is perfectly regular (see Koen 2006, 2010 for a description of the irregularly sampled case). The Nyquist frequency of regularly sampled data is half the sampling frequency, and is defined as

$$f_{\text{Ny}} = f_S/2 = 1/(2\Delta t), \tag{1}$$

where Δt is the sampling interval. The time stamp of an observation t_j, can therefore be written as

$$t_j = t_0 + j\Delta t \tag{2}$$

for an arbitrary (fixed) start time t_0.

In order to resolve Nyquist aliases, some modifications to the sampling must be made.

3 ORBITAL MODULATION OF THE SAMPLING

In this section, we demonstrate that the super-Nyquist asteroseismology method from Murphy et al. (2013a), which utilizes the periodic modulation of the sampling due to the orbit of the satellite, will not be viable for resolving Nyquist ambiguity with *TESS*. The full mathematical foundation for this analysis was presented by Murphy et al. (2013a), and so the interested reader is referred there. Given the null result here, we restrict this discussion to only the most relevant points.

The super-Nyquist asteroseismology method as applied to *Kepler* relies on the substantial modification of the time-stamps due to orbital motion. Since *Kepler* orbits the Sun with a semimajor axis, a, of 500 light-seconds, light arrives at the telescope early or late, compared to the Solar system barycentre. Thus, when the observation times are corrected to the arrival time at the Solar system barycentre, a periodic modulation is imprinted. The time delay was described by Murphy et al. (2013a, equation 11 there) as

$$\delta t(t) = \frac{a}{c} \cos\beta \cos\{\lambda_\odot(t) - \lambda\}, \tag{3}$$

where λ and β are the ecliptic longitude and latitude of the *Kepler* field. The $\cos\beta$ term reduces the effective Rømer delay,

$$\tau = \frac{a}{c} \cos\beta, \tag{4}$$

Table 1. Parameters for *TESS* 30-min sampling.

Parameter	Value	Units
τ	9.26×10^{-6}	d
Δt	2.08×10^{-2}	d
ω_S	$3.02 \times 10^{+2}$	rad d^{-1}
Ω_{orb}	4.59×10^{-2}	rad d^{-1}

to ± 200 s, which is still a substantial fraction of the ~ 1770 s sampling interval of *Kepler* LC mode.

Murphy et al. (2013a) showed that the periodic modulation of the sampling causes aliases in the Fourier transform to become multiplets, while the real angular oscillation frequency, $\omega_R \equiv 2\pi f_R$, remains a single peak. The central components of each multiplet are found at the anticipated alias frequencies, that is, at $n\omega_S \pm \omega_R$, where ω_S is the sampling frequency and n is an integer, while the additional components of the multiplets are separated from the central component by integer multiples of the angular orbital frequency ($\Omega_{\text{orb}} \equiv 2\pi/P_{\text{orb}}$), that is, at $n\omega_S \pm \omega_R \pm m\Omega_{\text{orb}}$. The amplitudes of the mth components of the multiplet with respect to the central peak are determined from the ratio of the Bessel coefficients $J_m(n\omega_S\tau)/J_0(n\omega_S\tau)$.

Application of equation (4) to *TESS* yields a maximum Rømer delay of $\tau \simeq 0.8$ s, if the eccentricity of the orbit is neglected. Since *TESS*'s orbit is inclined to the ecliptic, the relevant angle in equation (4) is no longer the ecliptic latitude, but the angle between the satellite's orbital plane and the target, which we call β', and which still has the minimum value of $0°$. The *TESS* full-frame images will have a cadence approximately equal to the *Kepler* LC mode, thus the amplitudes of the non-central components of the alias multiplets will be reduced by a factor of $\tau_{\text{Kepler}}/\tau_{\text{TESS}} = 200/0.8 = 250$. Relevant parameters of the *TESS* 30-min sampling are given in Table 1.

By computing the Bessel coefficients $J_m(n\omega_S\tau)$ for $n = [0, \ldots, 7]$ and $m = [0, \ldots, 3]$ we can evaluate the multiplet structure for the first $2n + 1 = 15$ Nyquist aliases, and determine whether these multiplets will be detectable in the Fourier transform of typical *TESS* observations of classical pulsators. The small value of τ for the *TESS* orbit causes the Bessel coefficients to change very slowly with $\xi \equiv \omega\tau$, as indicated in Fig. 1. The implications are that the Nyquist aliases are self-similar and cannot be used to resolve Nyquist ambiguity, even in the most favourable case of a target in the orbital plane (i.e. with $\beta' = 0$). The amplitudes of the first sidelobes of the multiplets are tiny, as given in Table 2, and more distant sidelobes (higher m) are completely negligible (see Fig. 1 caption). Although the first sidelobes do become detectable in higher order aliases (higher n), the self-similarity of neighbouring aliases does not permit distinction between them, and the real peak cannot be identified.

An approximate anticipated visibility of the sidelobes observed by *TESS* can be calculated. This example uses δ Sct stars, which are classical pulsators with low-order p modes and periods in the range of ~ 15 min–5 h, but similar examples can be constructed for other classes of pulsating stars with coherent oscillations. The first pair of Nyquist aliases for a star in the ecliptic plane will have sidelobes with maximum amplitudes of $[J_1(\omega_S\tau)/J_0(\omega_S\tau) =]$ 0.135 per cent of that of the central component. Given an estimated standard deviation of relative flux of 200 ppm h$^{-1/2}$ for a 10th magnitude star (Sullivan et al. 2015), and fields of 27.4 d = 657.6 h (neglecting the central downlink gap), then an optimistic noise floor of 8 ppm will apply. While there are some *Kepler* δ Sct stars with
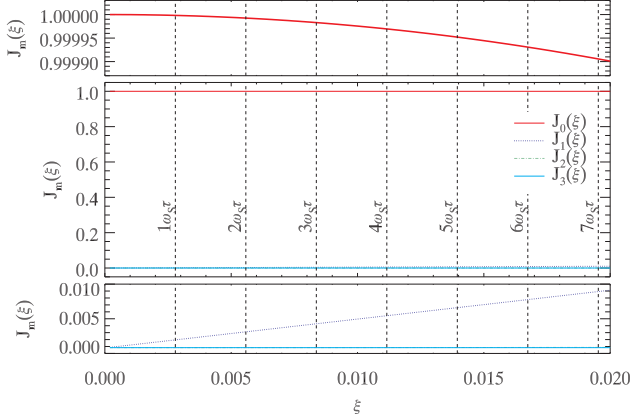
Figure 1. The Bessel coefficients $J_m(\xi)$ with $m = [0, \dots, 3]$ for $\xi = [0, \dots, 0.02]$. The vertical lines show $\xi = n\omega_S\tau$ with $n = [0, \dots, 7]$, at which the window spectrum has sharp but small multiplet peaks. The centre panel shows all Bessel coefficients, while the top and bottom panels zoom in to show the variation of $J_0(\xi)$ and $J_{1,\dots,3}(\xi)$, respectively. The highest values of the coefficients of $J_2(\xi)$ and $J_3(\xi)$ in this range are 5.0×10^{-5} and 1.6×10^{-7}, respectively.

Table 2. Amplitude ratios of the first sidelobes of an alias multiplet ($m = 1$) to the central component ($m = 0$), as a function of the alias identification (of the form $n\omega_S \pm \omega_R$), for *TESS* 30-min sampling. The amplitude ratios for negative values of n are identical to their positive values.

$|n|$	Amp.($m = 1$) / Amp.($m = 0$)
0	0.000 000
1	0.001 350
2	0.002 750
3	0.004 150
4	0.005 550
5	0.006 950
6	0.008 350
7	0.009 750

amplitudes of tens of mmag (e.g. KIC 9700322: Breger et al. 2011, Guzik & Breger 2011; KIC11754974: Murphy et al. 2013b), *Kepler* has shown that typical δ Sct stars have amplitudes on the order of 1 mmag (Balona & Dziembowski 2011), or ∼1 ppt of relative flux. The *TESS* passband is redder than that of *Kepler*, so oscillation amplitudes will be lower, but we assume amplitudes of 1 ppt for ease of calculation. Then, the maximum sidelobe amplitudes are of the order of 1 ppm for the first Nyquist alias, and only around 7 ppm for the fifth Nyquist alias (that is, at $\xi = 5\omega_S\tau$; see Table 2). Brighter stars have a lower noise floor, estimated to be as low as 60 ppm h$^{-1/2}$ (Sullivan et al. 2015). However, in reality the spectral window of the many different Fourier peaks in multiperiodic oscillators will contribute extensively to the noise level, and such sidelobes will remain undetectable.

Thus far, only the 30-min cadence of *TESS* has been discussed. The Bessel coefficients depend on the sampling frequency; therefore, the sidelobes of the alias multiplets will be much higher in the shorter cadence modes (Fig. 2). However, these modes also have higher Nyquist frequencies (4320 d^{-1} = 50 mHz for the 20-s cadence), and so there will be no Nyquist ambiguity in need of resolution.
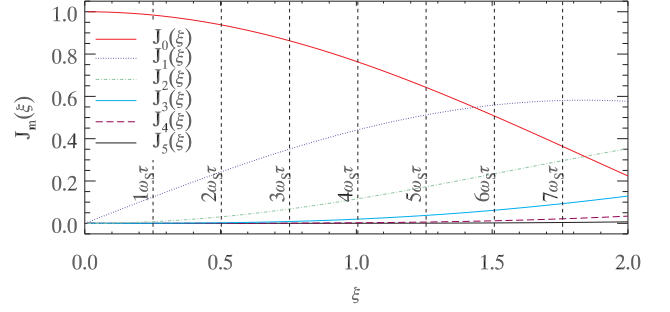

Figure 2. The Bessel coefficients $J_m(\xi)$ with $m = [0, \dots, 5]$ for $\xi = [0, \dots, 2.0]$ for the *TESS* 20-s cadence where $\omega_S = 2.71 \times 10^4$ rad d^{-1}. The vertical lines show $\xi = n\omega_S\tau$ with $n = [0, \dots, 7]$, at which the window spectrum has sharp multiplet peaks with significant sidelobe amplitudes, which could be used to distinguish real peaks from their Nyquist aliases.

In the next section, we present a promising alternative approach that will enable Nyquist ambiguity to be resolved in all observing modes, and that will additionally benefit the main mission in the discovery of exoplanets.

4 OFFSETTING THE SAMPLING

If the sampling interval is irregular, or an offset is introduced, Nyquist aliasing can be alleviated, as illustrated in Fig. 3. The data shown there are simulated *TESS* data with 30-min sampling, for a monoperiodic star oscillating at 9.71 d^{-1} (=112.4 μHz).[1] Halfway through the data set, a single offset of half a cadence (15 min) is introduced, and thereafter the cadence remains fixed at 30 min. That is, the time stamps in the second half of the data set are now expressed as

$$t_j = t_0 + (j + \epsilon)\Delta t, \tag{5}$$

where ϵ is the introduced offset that in this case is equal to 0.5. The offset causes the first Nyquist alias to be in antiphase with the observations, allowing it to be easily distinguished from the real peak.

The anticipated *TESS* data are of longer duration than those shown in Fig. 3, and the proposed sampling offset would be introduced after each downlink, which are of 'no more than 16 h' (Ricker et al. 2015). Therefore more realistic 27-d simulations were created with a central gap during which an offset is introduced. The gap was set at 0.8 d, corresponding to a pessimistic 19-h duration, but the exact length is unimportant. The Fourier transform of those simulations for a monoperiodic star oscillating at an input frequency of $f_{in} = 9.71$ d^{-1} are shown in Fig. 4, for values of $\epsilon = 0$, 0.5 and 0.213. The latter value was chosen to be approximately intermediate between the in-phase ($\epsilon = 0 \equiv 1$) and antiphase ($\epsilon = 0.5$) cases, but not have a simple relationship with either 0.5 or 1.

It can be seen in the top panel of Fig. 4 that if no offset is introduced, the Nyquist aliases all have equal amplitudes and the identification of the real peak is totally ambiguous. However, introduction of an offset of $\epsilon = 0.5$ causes the Nyquist aliases at $f_S \pm f_{in}$ to have amplitudes lower than the input peak. In this way, the Nyquist ambiguity has been resolved and the input frequency can be recovered. But notice the alias peak near 87 d^{-1} (≈1000 μHz), whose amplitude is still equal to that of the input frequency. This alias

---

[1] The oscillation frequency was chosen to not have a simple integer relationship with the sampling frequency.
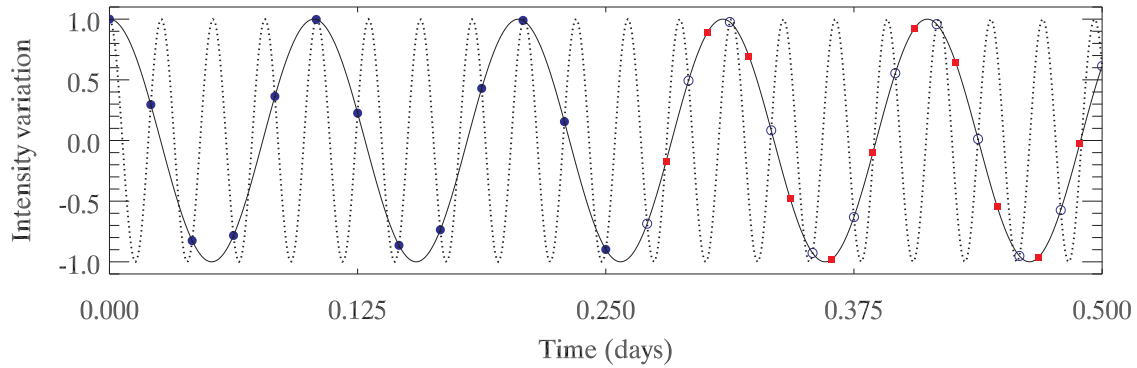
Figure 3. Simulated *TESS* data with 30-min sampling are shown as blue circles. Halfway through the observations an offset is introduced, altering the sampling to the red squares, after which the cadence remains a strict 30 min. The sampled oscillation has a frequency of 9.71 d^{-1} (solid line), which has a corresponding Nyquist alias at 38.29 d^{-1} (dashed line). If the cadence had remained strictly regular at 30 min then the real peak and its alias would have fitted the data equally well, but due to the offset only the real peak remains a good fit.
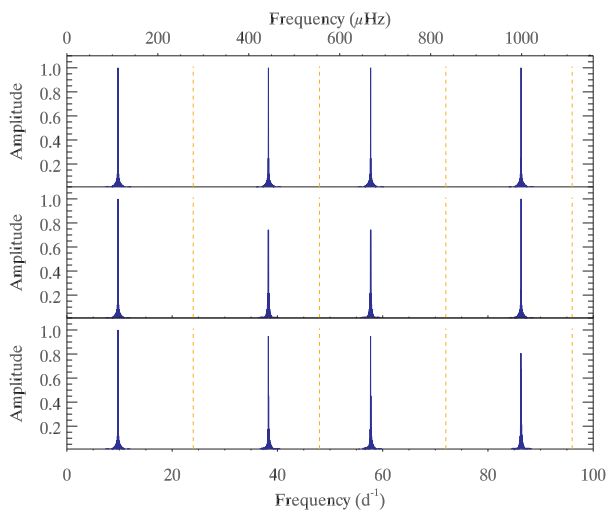

Figure 4. Fourier transforms for three different values of the offset parameter ϵ: top = 0.0, middle = 0.5, bottom = 0.213. Dashed orange lines are drawn at integer multiples of the Nyquist frequency, $f_{\rm Ny} = 24.0$ d^{-1}. The input frequency, $f_{\rm in}$, is 9.71 d^{-1}.

Figure 5. Fourier transform of 27 d of simulated *TESS* data with an offset of $\epsilon = 0.213$. Dashed orange lines are drawn at integer multiples of the Nyquist frequency ($=24$ d^{-1}). The input frequency, $f_{\rm in} = 9.71$ d^{-1}, has the highest amplitude up to a frequency of 230 d^{-1}, where a pair of aliases have similar amplitudes.

can only be discarded if we have an external physical constraint with which to select the real peak. In practice, this tends to be the case, because here the real and ambiguous alias peak are an order of magnitude different in frequency. However, the bottom panel of Fig. 4 shows that there is no need; an offset that is not a simple fraction of 0.5 or 1.0 will produce a series of aliases whose amplitudes are all lower than that of the input frequency, out to much higher frequency in the Fourier transform (see Fig. 5). The Nyquist ambiguity can then be considered completely resolved. The reason is twofold: (1) any astrophysical target for which ambiguity at such high frequency could be an issue would presumably have been proposed for the shorter cadence slots anyway; and (2) oscillation frequencies so much higher than the sampling frequency will have severe amplitude attenuation (a factor ∼10 reduction at 230 d^{-1}) and will most likely be unsuitable for study (see Section 5.1).

5 SUPER-NYQUIST ASTEROSEISMOLOGY

With the introduction of a suitable offset, real peaks can be distinguished from aliases even when those real peaks exceed the Nyquist
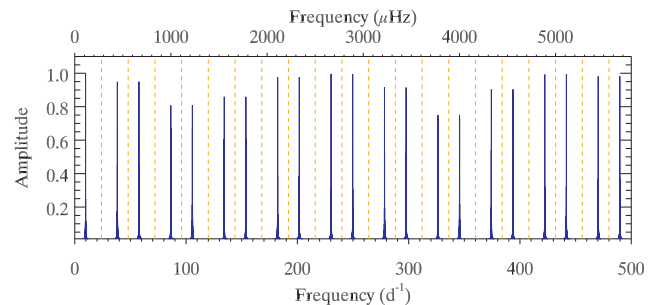
frequency. In Fig. 6, the general case is shown, where the star is multiperiodic and the input oscillations are distributed above and below the Nyquist frequency, at 9.710, 26.240 and 41.033 d^{-1}. These input oscillations were given random phases. Noise was added to the simulated data at a level anticipated for a 13th magnitude star.

The input oscillations are entirely recoverable by selecting the peak with the highest amplitude from the set of Nyquist ambiguities for each mode. Even for this 13th magnitude star, the amplitude differences in the bottom panel of Fig. 6 are significant to 10σ. Therefore, random noise spikes will not push an alias to an amplitude higher than the real peak.

Close inspection of Fig. 6 provides insight on the optimal offset for the purpose of distinguishing aliases. While amplitude differences are still significant for the 1.66 and 5.00-min offsets, it is clear that the 9.27-min offset is more favourable. The reasons are as follows. For the 1.66-min offset, the phase difference between the true peak and its alias has had little time to accumulate. An offset of 5.00 min, i.e. 1/6 of the 30-min cadence, trebles the available accumulation time, but it is preferable to avoid simple fractions of a cadence. The 9.27-min offset was chosen to not be a simple fraction and to be roughly intermediate between the fractional cadences of 0.0 and 0.5 discussed in the previous section. The amplitude differences are much larger as a result, as is shown in the next subsection.
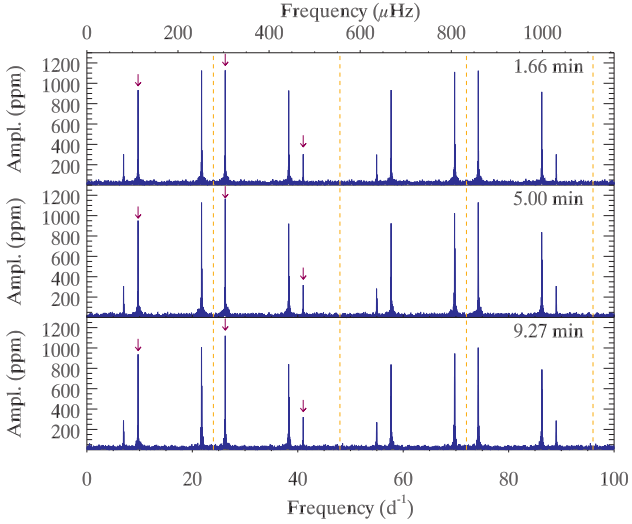
Figure 6. Fourier transform of 27 d of simulated *TESS* data with different values of the offset, ϵ. Dashed orange lines are drawn at integer multiples of the Nyquist frequency (=24 d^{-1}). The input frequencies, identified with arrows, are 9.710, 26.240 and 41.033 d^{-1}. They are distinguishable from their aliases by their higher amplitudes. The top, middle and bottom panels have offsets of 1.66, 5.00 and 9.27 min, respectively, which are equal to fractional cadences of $\epsilon = 0.0556$, 0.1667 and 0.3090.

5.1 Amplitude reduction of real and alias peaks

The effect of sampling on oscillation amplitudes as applied to *Kepler* data was described in detail by Murphy (2014). The amplitude reduction due to undersampling is a sinc function (Chaplin et al. 2011; Murphy 2012):

$$\mathcal{A}_{\mathrm{obs}} = \mathcal{A}_{\mathrm{in}} \, \mathrm{sinc}(\pi/x), \tag{6}$$

where x is the number of data points per oscillation cycle. This amplitude reduction is illustrated in Fig. 7.

In this work, the amplitudes of greatest interest are those of the aliases with respect to the real peak. The aliases come in pairs of the same amplitude, at frequencies of $nf_{\mathrm{S}} \pm f_{\mathrm{R}}$, where f_{S} and f_{R} are the sampling and 'real' oscillation frequency, respectively, and n is an integer coefficient. In Fig. 8, the ratios of the measured
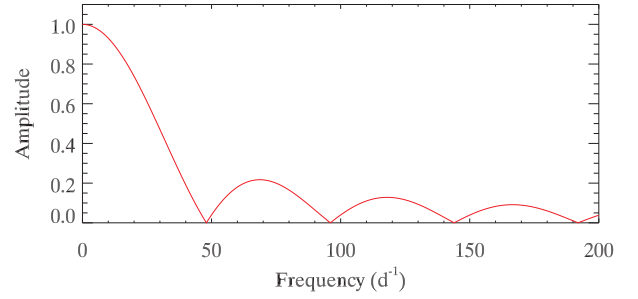

Figure 7. Measured amplitude in arbitrary units as a function of frequency, for *TESS* data with a sampling frequency of 48 d^{-1}. The input amplitude was 1.0 on this scale.

alias amplitudes, $\mathcal{A}(nf_{\mathrm{S}} \pm f_{\mathrm{R}})$, to the measured amplitude of the real peak, $\mathcal{A}(f_{\mathrm{R}})$, are shown as a function of the sampling offset, ϵ. The ratios were determined by simulating 1000 artificial *TESS* light curves of 27 d, with added noise, a central gap of 0.8 d, and a (uniformly) randomly generated ϵ for each light curve. The light curves were of a monoperiodic oscillator, each with a different oscillation frequency drawn from a uniform random distribution between 0.0 and 100.0 d^{-1}. The outcome is independent of those oscillation frequencies; the only important factors are n and ϵ. The functional form of the amplitudes in Fig. 8 is

$$\frac{\mathcal{A}(nf_{\mathrm{S}} \pm f_{\mathrm{R}})}{\mathcal{A}(f_{\mathrm{R}})} = |\cos(n\pi\epsilon)|. \tag{7}$$

It is easily seen from equation (7) and Fig. 8 that aliases at $nf_{\mathrm{S}} \pm f_{\mathrm{R}}$ will have the same amplitudes as the real peak at f_{R} if $\epsilon = i/n$, where i is an integer. Since both i and n are integers, simple fractions for ϵ are best avoided so that we can distinguish aliases from real peaks. Ideally, we would choose ϵ to be irrational, e.g. as $1/\pi$, but in practice ϵ is best chosen randomly. Specifically, *TESS* should return to observations as soon as it is ready, and should not wait in an attempt to return to perfect cadence. The most important distinction to be made is between the first alias pair ($n = 1$) and the real peak, since these are closest in frequency. Hence, if ϵ were carefully selected, values nearer to (but not equal to) 0.5 would be preferable to those nearer to 0.0 ($\equiv 1.0$).
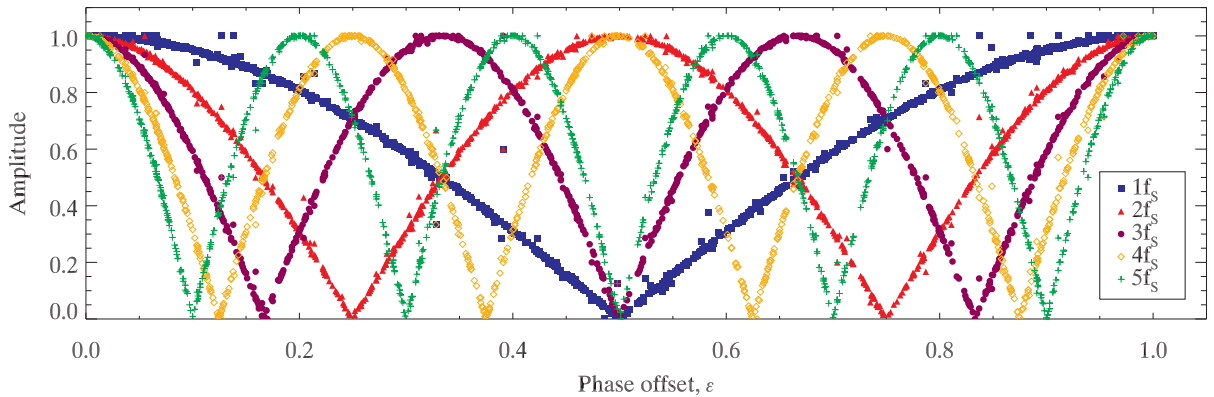

Figure 8. Amplitude ratios of alias peaks at $nf_{\mathrm{S}} \pm f_{\mathrm{R}}$ to real peaks at f_{R}, for integer $n = [1, \dots, 5]$. Aliases have amplitudes below their corresponding real peak, as long as ϵ is not a simple fraction. Noisy data contribute some scatter. Based on 1000 simulated light curves.
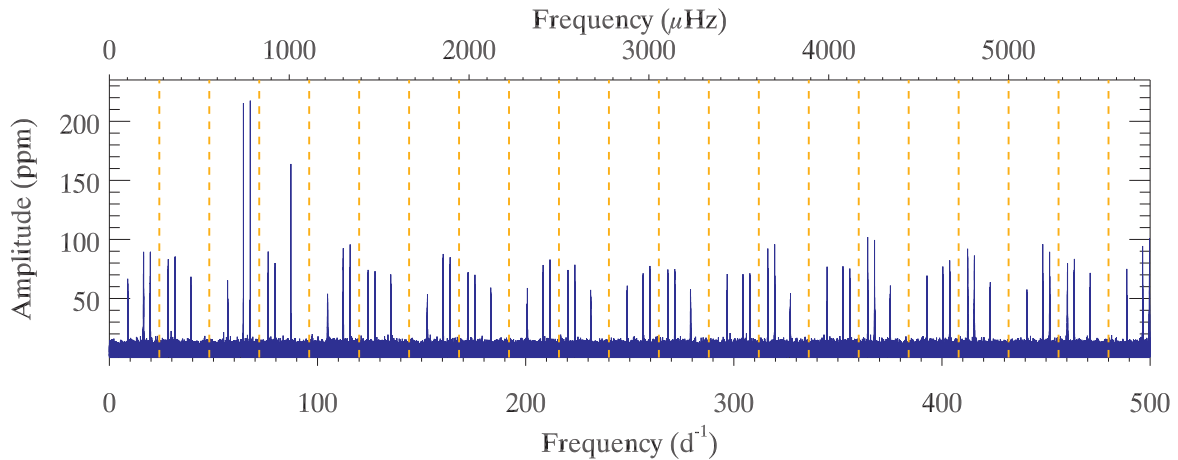
Figure 9. Fourier transform of 351 d of simulated *TESS* data, representative of the continuous viewing zone. The value of the offset, ϵ, is randomized every orbit. Dashed orange lines are drawn at integer multiples of the Nyquist frequency ($=24$ d^{-1}). The input frequencies at 64.4, 67.7 and 87.2 d^{-1} are completely recovered. The noise, corresponding to the prediction for a 15th magnitude star, has no effect on the ability to apply the method.

5.2 Other cadences

Carefully planned offsets could be inserted into the shorter cadence observations to achieve the same effect. The 2-min cadence is only six times longer than the 20-s cadence, and so the introduction of a suitable offset to that 2-min cadence could push its effective Nyquist frequency to roughly the same value as that of the 20-s cadence. This does not relieve the amplitude reduction effect due to undersampling (equation 6), so it will remain the case that 20-s sampling is warranted for high-frequency, low-amplitude oscillators such as white dwarfs. It is noteworthy that if a random offset is introduced for the purposes of the 30-min full-frame images, then the shorter cadences will automatically benefit from the same offset, though the fractional cadence of that offset will of course differ according to the length of the cadence considered.

Other photometric data sets can supplement *TESS* and *Kepler* data to resolve Nyquist ambiguities. For instance, the SuperWASP (Pollacco et al. 2006) and KELT (Pepper et al. 2007) data have random sampling, and oscillations can be detected at frequencies much higher than the mean sampling frequency. This is exemplified by the discovery of high-frequency oscillators in SuperWASP data (Holdsworth et al. 2014), which included rapidly oscillating Ap stars and the fastest δ Sct pulsator known.

5.3 Application to the continuous viewing zone

Some parts of the sky will be observed for more than 27 d. The *TESS* continuous viewing zones at the ecliptic poles will be observed for 351 d each. If the return to cadence is imperfect every time, that is, some random value of ϵ is implemented, then super-Nyquist asteroseismology is made easier. An example is provided in Fig. 9. The amplitude of the real peaks are at least twice those of the aliases, making the real peaks easy to identify, even when they have frequencies greater than the sampling frequency. Those amplitudes are still heavily reduced because the exposure time is longer than the pulsation period. The actual input amplitudes for the real peaks at 64.4, 67.7 and 87.2 d^{-1} were 1000, 1000 and 2000 ppm, respectively, and so the amplitude reduction shown in Fig. 7 is observed.

6 CONCLUSIONS

The short light-travel time across the *TESS* orbit causes only a small Rømer delay. The resulting modulation of the sampling interval over the orbital period is insufficient to produce detectable multiplets out of the Nyquist aliases in 30-min *TESS* full-frame images.

However, the Nyquist limits of all *TESS* cadences can be raised by introducing a sampling offset while the spacecraft performs a data downlink. Providing that the time of return to observations after downlink is not an integer number of cadences since the last observation, Nyquist ambiguities can be resolved. It was shown that an offset from perfect cadence with no simple integer relationship to a full cadence is preferable. Observing time can be recouped from the downlink event by implementing this proposed offset, because for the application to the full-frame images, the telescope need not wait for the observing gap to reach an integer multiple of 30 min in duration.

Application to the continuous viewing zone yields even more straightforward identification of the real peaks, because the amplitudes of the aliases are more strongly reduced as a result of several introduced sampling offsets.

Sampling offsets are also important to the main goal of the mission. With the huge number of transiting events that *TESS* will detect, it is inevitable that some celestial orbital periods will be an integer (or near-integer) multiple of the sampling interval, which will lead to poor transit phase coverage. Offsetting the sampling after downlink will alleviate this and open up additional opportunity for transit timing variations for the very short-period planets, or for planets in the continuous viewing zone.

The major consequence of this work is that thousands more stars will be opened up for asteroseismic study.

REFERENCES

Balona L. A., Dziembowski W. A., 2011, MNRAS, 417, 591
Breger M. et al., 2011, MNRAS, 414, 1721
Chaplin W. J. et al., 2011, ApJ, 732, 54
Guzik J. A., Breger M., 2011, Commun. Asteroseismol., 162, 62
Holdsworth D. L. et al., 2014, MNRAS, 439, 2078
Howell S. B. et al., 2014, PASP, 126, 398
Koch D. G. et al., 2010, ApJ, 713, L79
Koen C., 2006, MNRAS, 371, 1390
Koen C., 2010, MNRAS, 401, 586
Murphy S. J., 2012, MNRAS, 422, 665
Murphy S. J., 2014, PhD thesis, Univ. Central Lancashire
Murphy S. J., Shibahashi H., Kurtz D. W., 2013a, MNRAS, 430, 2986
Murphy S. J. et al., 2013b, MNRAS, 432, 2284
Pepper J. et al., 2007, PASP, 119, 923
Pollacco D. L. et al., 2006, PASP, 118, 1407
Ricker G. R. et al., 2015, J. Astron. Telesc. Instrum. Syst., 1, 014003
Sullivan P. W. et al., 2015, ApJ, 809, 77

This paper has been typeset from a TEX/LATEX file prepared by the author.